water

MDPI

Article

Synthesis, Characterization, and Application of Pt/PtO_2-TiO_2/SiO_2 Materials on a Continuous Flow Packed Bed Microreactor for Enhanced Photocatalytic Activity under Sunlight

Carolina de Araújo Gusmão [1,*], Laura Teixeira Borges [1], Priscila Hasse Palharim [1], Larissa Otubo [2], Orlando Rodrigues [2], Douglas Gouvea [3], Bruno Ramos [3] and Antonio Carlos Silva Costa Teixeira [1,*]

[1] Research Group in Advanced Oxidation Processes (AdOx), Department of Chemical Engineering, Escola Politécnica, University of São Paulo, São Paulo 05508-060, SP, Brazil
[2] Instituto de Pesquisas Energéticas e Nucleares, IPEN/CNEN, São Paulo 05508-060, SP, Brazil
[3] Laboratory of Ceramic Processes (LCP), Department of Material Engineering, Escola Politécnica, University of São Paulo, São Paulo 05508-060, SP, Brazil
* Correspondence: carolina.argusmao@usp.br (C.d.A.G.); acscteix@usp.br (A.C.S.C.T.); Tel.: +55-81-9-9956-4698 (C.d.A.G.)

Abstract: The present work aimed at the development of Pt-TiO_2/SiO_2 materials applied to the degradation of a pharmaceutical pollutant in a fixed-bed microreactor in continuous mode. First, a wide investigation of the optimal platinum content in TiO_2/SiO_2 was carried out based on extensive characterization through XRD, DRS, SEM, TEM, and XPS techniques. For the content range studied, no significant changes were observed in the crystallinity of the material, with peaks related to the anatase phase and PtO_2 in the diffractograms. SEM images combined with EDS spectra indicated the presence of platinum and a large heterogeneity in the particles. MET analyses showed PtO_2 nanoparticles in close contact with TiO_2, allowing the formation of a type II heterojunction. XPS showed platinum in the 0 and +4 oxidation states, suggesting that platinum metal and PtO_2 are both present. Regarding the degradation experiments, the optimal catalyst achieved 81% degradation of acetaminophen for a residence time of 1 h, while the catalyst without platinum reached only 27% degradation. The catalyst activity dropped from 81 to 57% in 2 h and remained stable for six reuse cycles. Increasing the inlet flow rate and concentration reduced the pollutant degradation although there was an increase in the reaction rate. Finally, a photocatalytic mechanism was proposed in which a type II heterojunction was developed, with generation of hydroxyl radicals by the positive holes in the VB of TiO_2 as well as superoxide radicals by the electrons in the CB of PtO_2.

Keywords: photocatalysis; microreactor; doped TiO_2; emerging pollutants; solar light

Citation: Gusmão, C.d.A.; Borges, L.T.; Palharim, P.H.; Otubo, L.; Rodrigues, O.; Gouvea, D.; Ramos, B.; Teixeira, A.C.S.C. Synthesis, Characterization, and Application of Pt/PtO_2-TiO_2/SiO_2 Materials on a Continuous Flow Packed Bed Microreactor for Enhanced Photocatalytic Activity under Sunlight. *Water* **2022**, *14*, 3864. https://doi.org/10.3390/w14233864

Academic Editor: John Zhou

Received: 20 October 2022
Accepted: 24 November 2022
Published: 27 November 2022

1. Introduction

Different classes of pollutants of emerging concern are continuously introduced into soil, groundwater, and water ecosystems at appreciable concentrations. Hygiene products, therapeutic drugs, hospital waste, and pharmaceutical industry waste are the main sources of these pollutants [1–4]. The presence of pharmaceuticals in water, for instance, can affect water quality, posing a threat to the aquatic ecosystem as well as to human health [4–7]. Therefore, this issue is a public health concern, as there is still little knowledge about the chronic effects associated with long-term contact/ingestion of the mixture of this type of compounds [8]. Acetaminophen (paracetamol) is an example of a popular analgesic that can be found in effluents and surface water bodies at concentrations ranging from ng L^{-1} to μg L^{-1} [9–12].

Polluted water can be treated by physical, chemical, and biological processes; however, in many cases, conventional treatments are not able to degrade pollutants of emerging

concern to levels acceptable or required by law [4]. Therefore, technologies based on advanced oxidation processes (AOPs) have been shown to be effective in the oxidation of various organic and inorganic compounds [13]. Among these processes, heterogeneous photocatalysis is a technology based on the use of semiconductors, which are activated under light irradiation, including solar radiation [14,15]. When a semiconductor is exposed to light with energy equal to or greater than its band gap energy, electrons (e^-) are excited, and holes (h^+) are formed. Subsequently, several reactions can be initiated once the photogenerated charge carriers (e^-/h^+) are formed and move from the bulk to the semiconductor surface [1,16,17]. Titanium dioxide (TiO_2) is the most widely used semiconductor due to its low cost, photochemical stability, low toxicity, and high photoactivity. Nonetheless, TiO_2 presents high recombination of photogenerated e^-/h^+ pairs and limited absorption in the ultraviolet region as main drawbacks [18,19].

To overcome these disadvantages, the doping of TiO_2 catalysts with metals such as Pt, Ag, Pd, Cu, Cr, and Fe has been studied [20–24]. The doping process can promote the reduction of TiO_2 band gap energy as well as increase the photocatalytic activity [25,26]. Furthermore, modification of the TiO_2 structure with metals can lead to the formation of the Schottky barrier [24,27–29], whereby the photoexcited electrons of the TiO_2 conduction band can be collected by a metal with Fermi level lower than that of TiO_2. Thus, these metals, especially Pt, can act as electron traps to enhance charge separation, suppressing recombination and subsequently allowing interfacial electron transfer to other electron acceptors [30,31]. However, an optimal metal content in the photocatalyst is required so that the metallic nanoparticles can act as charge recombination centers [24,27]. Murcia et al. (2013) [1] evaluated the effect of different Pt loadings on Pt/TiO_2 photocatalysts and found that increasing Pt concentration resulted in agglomeration of these particles and in a lower metal platinum content on the surface of TiO_2 [32].

Pt species can exist as Pt^0, Pt^{2+}, and Pt^{4+}; however, there are still few studies reporting the presence of oxidized Pt, such as PtO or PtO_2 [31]. According to Parayil et al. (2013) [2], the heterojunction formed between TiO_2 and PtO_2 can indeed decrease electron–hole recombination since Pt or PtO_2 can effectively trap electrons [31]. Ren et al. (2017) [3] reported the deposition of Pt/PtO nanodots in the TiO_2 lattice with high surface area, which led to enhanced hydrogen production [33]. The authors claimed that the platinum nanoparticles act as photogenerated charge carrier separators, while the coexistence of Pt and PtO provides more active sites, and PtO inhibits the hydrogen back reaction, which is undesirable for H_2 production [33].

The type of photocatalytic reactor used in the process is also a determining factor. The fixed-bed reactor, for example, has many advantages such as ease of residence time control and operation. Additionally, continuous flow reactor operation offers increased heat transfer, more efficient mixing of reactants, and greater mass transfer compared to conventional batch reactors [34,35]. To make the fixed-bed reactor feasible, silica gel can be used as a support for TiO_2 to prevent particle leaching since the silica coupled to TiO_2 would have a micrometer size, while the pure semiconductor material has a nanometric scale [19,36]. Although the synthesis of TiO_2/SiO_2 has already been studied [19], coupling with Pt is rarely reported, especially for water treatment process purposes.

Although platinum-containing TiO_2 has been explored by different studies [2,3,33,37], there are no previous reports regarding TiO_2/SiO_2 coupled to PtO_2 and Pt simultaneously. In addition, to the best of our knowledge, no previous works have focused on the photocatalytic performance of TiO_2-based materials in continuous fixed-bed reactors for pharmaceutical degradation. Other fundamental contributions, including (i) determining the positions of valence and conduction band potentials and (ii) in-depth investigation about the reaction mechanism for $Pt\text{-}PtO_2\text{-}TiO_2/SiO_2$ catalysts based not just on experimental assays with radical scavenging agents but also on characterization analyses of steady-state photoluminescence spectroscopy and electron spin resonance spectroscopy through spin trapping technique, have not been addressed as regards $Pt\text{-}TiO_2/SiO_2$ applied to continuous fixed-bed reactor and are discussed here for the first time.

2. Materials and Methods

2.1. Materials

Titanium isopropoxide IV (TTIP, 97%), silica-gel 63–200 μm, and $H_2PtCl_6 \cdot 6H_2O$ (>99%) were purchased from Sigma-Aldrich (St. Louis, MO, USA). Nitric acid (HNO_3, 65%), acetaminophen (ACT, 96%), methanol (>99%), and 5,5-dimethyl-1-pyrroline N-oxide (DMPO, >97%) were supplied by Merck (Darmstadt, Germany). These chemicals were used as received without further purification. Ultra-pure water (18.2 MΩ cm) from a Milli-Q®® system (Millipore, Burlington, MA, USA) was used in the preparation of the solutions used in the synthesis procedure and photodegradation tests.

2.2. Synthesis and Preparation of the Photocatalysts

The synthesis of pure and Pt-doped TiO_2/SiO_2 was performed using an acidic sol-gel procedure based on the adaptation of a method previously developed by Gusmão et al. (2021) for the synthesis of Ag-TiO_2/SiO_2. First, 8.4 mL of TTIP was added to a 1 mol L^{-1} solution of HNO_3 with vigorous stirring. After 1 h, the pH was raised to 2.0 by adding NaOH, and the platinum precursor ($H_2PtCl_6 \cdot H_2O$) was added in a predetermined amount according to the Pt content in the final material. Subsequently, the formed gel was irradiated for 30 min under a UVC lamp for platinum photoreduction. Subsequently, silica gel was added in the 60%TiO_2:40%SiO_2 mass ratio. After 1 h, NaOH was added until the pH reached 3.0, and finally, the material obtained was transferred to dialysis membranes. After the pH of the supernatant reached neutral pH, the catalyst was dried at 80 °C for 48 h and calcined at 450 °C in a muffle furnace for 240 min.

2.3. Characterization Techniques

Scanning electron microscopy (SEM-FESEM JSM-7401F JEOL) coupled with energy dispersive spectroscopy (EDS),and high-resolution elemental mapping (Thermo Scientific NSS spectral imaging system, Waltham, MA, USA) were used to assess the particle size and morphology of the catalysts. A JEOL JEM-2100 equipment was used to obtain transmission electron microscopy (TEM) and high-resolution transmission electron microscopy (HRTEM) images; Pt-TiO_2/SiO_2 particles were dispersed in ethanol and placed in an ultrasonic bath for 30 min for this study. For the acquisition of crystalline structure information, such as crystalline phases and crystal size, X-ray diffraction technique was used in the range 2θ = 20–80° at a scan rate of 0.02° s^{-1} (D8 Focus—Bruker AXS, Billerica, MA, USA). The light-absorption properties of the catalysts were evaluated by diffuse reflectance spectroscopy (UV 2550, Shimadzu Co). The effective Pt content in the Pt-TiO_2/SiO_2 materials was calculated using X-ray dispersion energy (EDX) spectroscopy (NEX-RIGAKU). In order to assess the energy states of the elements on the photocatalytic surface, X-ray photoelectron spectroscopy (Thermo Scientific, K-Alpha, Al K 1486.6 eV, X-ray spot size of 400 m, 10–8 mBar) was applied. For this analysis, 5 mg of the Pt-TiO_2/SiO_2 catalysts were fixed on an aluminum strip, then degassed in an ultra-high vacuum (UHV) chamber at 25 °C. Electron paramagnetic resonance (EPR) spectroscopy, using a Bruker EMXplus operating in X-band at room temperature, was applied to evaluate unpaired electrons in the pure TiO_2/SiO_2 and Pt-TiO_2/SiO_2 materials. In addition, EPR analysis was also applied to elucidate the radical species involved in Pt-TiO_2/SiO_2-driven degradation assays using DMPO as the spin-trapping agent. Finally, photoluminescence spectra were used to evaluate the generation and recombination of photogenerated charges. Photoluminescence spectroscopy (PL) was assessed using a Horiba Yvon-Jobin Fluoromax-222 (Em/Exc; slit 1.0 nm) in the 350–700 nm region, equipped with a xenon lamp and a Peltier-cooled FL-123450 PMT detector.

2.4. Experimental Reaction Unit

To evaluate the photocatalytic activity of the materials, experiments were performed in a microstructured continuous flat plate photochemical reactor, prototyped by additive technique via 3D printing as described elsewhere [38]. Figure 1 shows a schematic illus-

tration of the experimental apparatus used in this work. For each degradation test, 0.4 g of Pt-TiO_2/SiO_2 catalyst was placed in the microreactor, which has a capacity of 3.0 mL. Subsequently, the reactor was closed at the top with a borosilicate glass window and sealed. Then, 60 mL of acetaminophen (ACT) solution was loaded into a syringe coupled with a precision syringe pump (11 Elite, Harvard Apparatus Ltd. Holliston, MA, USA) used to feed the reactor at a volumetric flow rate of 3 mL h^{-1}. The inlet ACT concentration was varied at different levels from 0.0067 to 0.33 mmol L^{-1}, according to those usually found in wastewater generated in the washing of tablet processing equipment in the pharmaceutical industry (1.0–50.0 mg L^{-1}). After reaching the adsorption-desorption equilibrium condition, photocatalytic assays were conducted using an HgI_2 light source (HPI-Plus Phillips Co., Amsterdam, the Netherlands). The irradiance at the reactor surface (76.0 × 26.0 cm) under these conditions was 4.2 mW cm^{-2}, and it was measured using a spectroradiometer (Luzchem, SPR-4002, Ottawa, Canada). The irradiance spectrum of the light source at the reactor is shown in Figure 1. Next, 0.5 mL samples were collected over time at the reactor outlet, filtered through a PVDF filter (13 mm, 0.45 µm) and analyzed by high-performance liquid chromatography (HPLC). The ACT concentration was quantified using an HPLC Shimadzu LC20 chromatograph, equipped with a C18 column (Prominent) and with a UV–vis detector (SPD20A). The mobile phase was methanol: water (25:75), with a flow rate of 1.0 mL min^{-1}, injection volume of 50 µL, and oven temperature of 35 °C. The detection wavelength was 243 nm, and the retention time was 7 min. The limits of detection and quantification of ACT were 0.08 and 0.24 mg L^{-1}, respectively. After carrying out the tests to select the material with optimal platinum content (pure TiO_2/SiO_2, 0.1%Pt-TiO_2/SiO_2, 0.25%Pt-TiO_2/SiO_2, 0.5%Pt-TiO_2/SiO_2, and 1%Pt-TiO_2/SiO_2), using a fixed ACT concentration of 0.033 mmol L^{-1}, an investigation of operational parameters, including acetaminophen input concentration and volumetric flow rate, was carried out. Finally, five consecutive reuse cycles were performed using the same material to assess its stability over time in the fixed-bed continuous photocatalytic reactor, also comparing the XRD, SEM, and TEM analyses for the fresh and reused material.

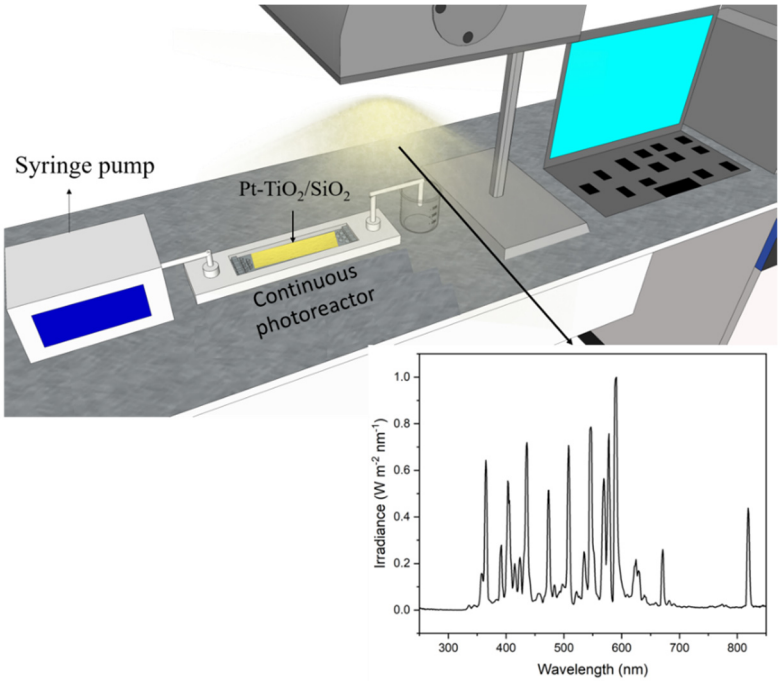

Figure 1. Schematic representation of the experimental apparatus, including the irradiance spectra measured at the reactor surface.

Degradation tests were evaluated with regard to steady-state ACT conversion, X (Equation (1)), and apparent reaction rate, r (Equation (2)). In these equations, C_0 and C_e

denote the steady-state inlet and outlet concentrations, respectively; v_0 is the flow rate of the ACT solution through the reactor, and m_{cat} is the mass of catalyst.

$$X = \frac{C_e - C_0}{C_e} \quad (1)$$

$$r = \frac{v_0\ (C_0 - C_e)}{m_{cat}} \quad (2)$$

3. Results and Discussion

3.1. Characterization

3.1.1. Crystal Phase and Surface Composition

Figure 2a shows the diffractograms of the catalysts synthesized with different Pt contents and the XPS spectra of selected samples. Regarding TiO_2, all materials presented peaks only referring to the anatase crystalline phase, with the most intense peaks at 2θ = 25.3, 37.5, 48, 55, and 63°, corresponding to the crystalline planes (011), (004), (020), (015), and (024), respectively, according to JCPDS card no. 96-720-6076 [39,40]. The absence of peaks corresponding to metallic platinum may indicate that the concentration of Pt nanocrystals is too low for XRD detection compared to that of the TiO_2 crystals [41]. For each material, the diffractograms showed relatively wide peaks, indicating low crystallinity as a result of the presence of silica gel as a TiO_2 support [19,40,42]. Meanwhile, the diffractogram of the platinum-containing materials showed two peaks referring to platinum dioxide (PtO_2) at 2θ = 21.8° and 28.5°, which correspond to (002) and (100) faces, respectively, according to JCPDS card no. 96-153-7412 [43,44]. PtO_2 is a p-type semiconductor that forms a highly stable Schottky barrier [43]. The increase in the platinum content led to an increase in the intensity of the peak referring to the PtO_2 phase.

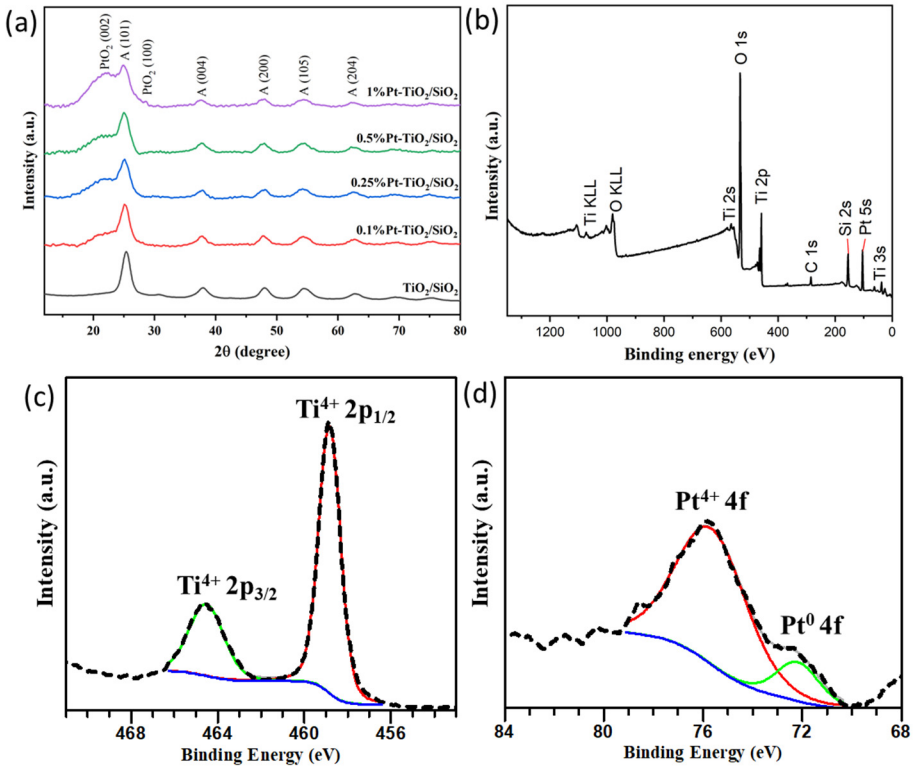

Figure 2. (**a**) XRD diffractograms of the synthesized materials, in which A corresponds to anatase; XPS spectra of 0.25%Pt-TIO_2/SiO_2: (**b**) XPS survey spectrum; (**c**) Ti 2p spectrum; (**d**) Pt 4f spectrum.

The average crystallite sizes of the TiO_2 and PtO_2 were calculated using the Scherrer equation (Equation (3)) [26,45,46], where D is the average crystallite size; β, the width of the

diffraction peak at half maximum height (FWHM); λ, the wavelength of the electromagnetic irradiation source used in the equipment; and θ, the Bragg diffraction angle. No significant changes were observed in the crystallite size of anatase and PtO_2 for materials containing different Pt contents, as shown in Table 1.

$$D = \frac{0.9 \times \lambda}{\beta \times \cos\theta} \quad (3)$$

Table 1. Theoretical and effective Pt contents, TiO_2 (anatase) crystallite size, and band gap energy of the prepared photocatalysts with different Pt-doping levels.

Sample	Effective Pt Content (wt%)	TiO_2 Crystallite Size (nm)	PtO_2 Crystalline Size (nm)	Band Gap Energy (eV)
TiO_2/SiO_2	0.00	6.1	–	3.20
0.1%Pt-TiO_2/SiO_2	0.15	4.8	2.3	3.21
0.25%Pt-TiO_2/SiO_2	0.35	4.9	1.3	3.20
0.5%Pt-TiO_2/SiO_2	0.60	5.4	1.3	3.22
1%Pt-TiO_2/SiO_2	1.10	5.7	1.2	3.19

According to Figure 2b–d, high-resolution XPS scans over the Ti 2p and Pt 4f spectra regions were used to verify the element compositions on the surface of the 0.25%Pt-TiO_2/SiO_2 material. The peak fitting of the high-resolution spectrum of Pt 4f showed two bands at 75.6 eV and 72.1 eV, corresponding to Pt^{4+} 4f and Pt^0 4f, respectively [43]. The band referring to Pt^{4+} was responsible for 84.95% of the molar fraction of Pt on the surface and Pt^0 for 15.05%, which evidences that Pt is predominantly at the 4+ oxidation state. This result is consistent with the XRD diffractograms of the platinum-containing materials, which showed peaks referring to PtO_2. Note that, according to XPS analysis, the presence of metallic platinum was also observed on the surface of the material although it could not be detected in XRD diffractograms. In addition, the Ti 2p doublet, which represents the Ti $2p_{1/2}$ and Ti $2p_{3/2}$ electrons, is shown in Figure 2c. Each signal was deconvoluted to just one band, centered at 461.0 eV and 466.0 eV, which correspond to the Ti (IV) ions of bulk anatase [43,47]. No bands referring to reduced Ti^{3+} species were observed, suggesting that platinum did not induce the formation of Ti^{3+} defects on the surface of the material [40].

The materials synthesized with different platinum contents were also analyzed by FRX. Table 1 shows the comparison between the nominal platinum content estimated by the amount of precursor added and the actual content from FRX analysis. It is worth mentioning that the content corresponds to platinum present in all oxidation states. In all materials, the effective platinum content was higher than nominal value, which may be related to losses in the synthesis step.

3.1.2. UV–Vis Spectroscopic Studies

DRS analysis was used to investigate the optical properties of TiO_2/SiO_2 and Pt-PtO_2-TiO_2/SiO_2 samples in the visible spectrum. Figure 3 shows the reflectance spectra of the synthesized materials. Furthermore, as shown in Table 1, the band gap energy of Pt-containing materials remained unchanged, indicating that the NPs were deposited only on the TiO_2 surface and must act as co-catalysts [31,33,48]. Furthermore, the reflectance of the Pt-doped sample in the visible range did not reach 100% even at 600 nm, a phenomenon previously attributed to the formation of structural color centers [49]. The light reflectance in the 400–600 nm wavelength range greatly increased as the Pt content in the material decreased, demonstrating that increasing platinum concentration increases visible light absorption [44,50]. As is widely known, two phenomena may be responsible for the visible light absorption of Pt-PtO_2-TiO_2: (1) the oxygen vacancy formed by the doped Pt^{4+} [31] and (2) the presence of PtO_2 species on the catalyst surface [50]. Since the induction of TiO_2 lattice defects was not observed from XPS analysis, as oxygen vacancy drives the formation of Ti^{3+} to maintain crystal charge neutralization, it is suggested that almost all visible light absorption of Pt-PtO_2-TiO_2/SiO_2 materials was driven by PtO_2 on the TiO_2 surface.

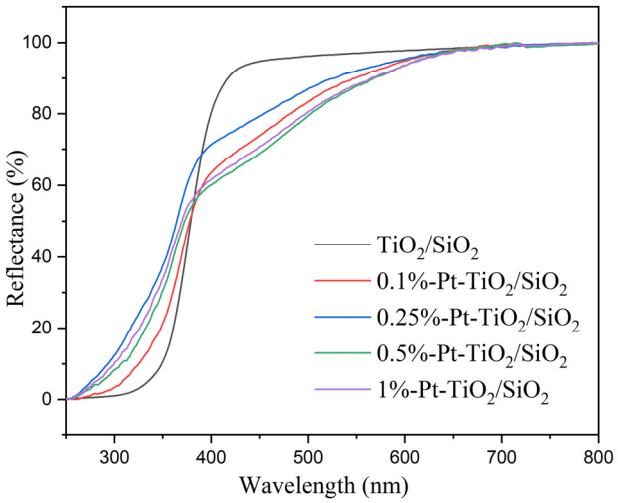

Figure 3. Diffuse reflectance spectra of the different synthesized materials.

3.1.3. Microstructural Analysis

Figure 4 shows SEM images of 0.25%Pt-TiO_2/SiO_2. The particles exhibited heterogeneous geometries, substantial variance in mean diameter size (Figure 4a), irregular shapes, and rough surfaces [40]. Figure 4a also shows a silica particle covered by TiO_2 nanoparticles. Figure 4b shows some heterogeneous TiO_2 agglomerates with an average size of 20 nm. Finally, Figure 4c shows a closer shot of the TiO_2 morphology. Some white circular platinum dots are observed, according to SEM-EDS, as shown in Figure 4d. It is observed that TiO_2 is both dispersed in silica and aggregated. In addition, EDS graphs support the presence of platinum in the material.

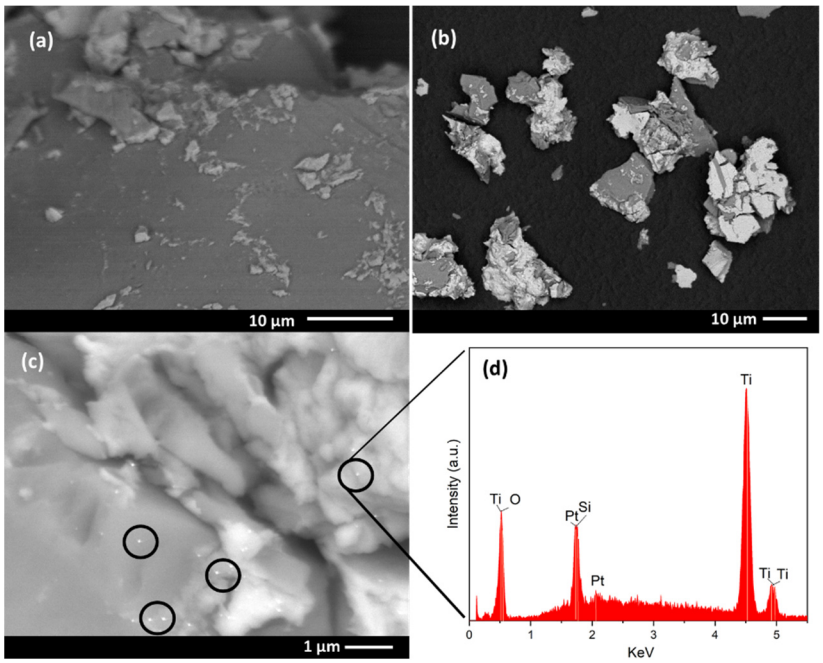

Figure 4. SEM images of 0.25%Pt-TiO_2/SiO_2.

The morphology and size distribution of TiO_2, PtO_2, and Pt^0 nanoparticles was evaluated by TEM and HRTEM images in Figure 5. Figure 5a,b show small PtO_2 particles, with an average size of 10 nm, adhered to the TiO_2 surface. The HRTEM images, shown in Figure 5c, showed lattice fringes of 2.22 and 2.23 Å, which are ascribed to the (002) crystallographic planes of PtO_2 [31,44]. It is worth noting that the d-spacing found is also

typical of the crystallographic plane (111) of metallic platinum (Pt^0) [43]. As the presence of Pt^0 was found in the XPS analysis of the material, it is suggested that the PtO_2 and Pt are well-mixed in a Pt/PtO_2 phase-junction [33]. In addition, an interplanar distance of 0.1 nm, related to (110) crystallographic plane of TiO_2, was also observed [19]. Furthermore, the HRTEM image of Figure 5d shows that TiO_2 is in close contact with PtO_2, which allows the formation of a heterojunction [31,51,52].

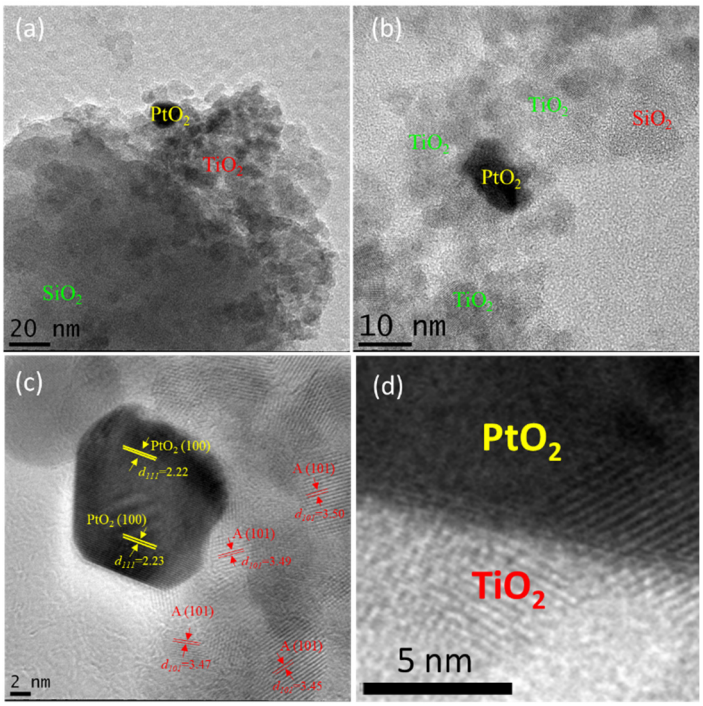

Figure 5. TEM and HRTEM images of 0.25%Pt-TiO_2/SiO_2.

3.2. Photocatalytic Tests

3.2.1. Effect of Pt Content

The performance of each composite material was evaluated by comparing its activity in relation to the degradation of a model pollutant, acetaminophen (ACT), in a continuous fixed-bed photoreactor, as described previously. Control experiments were performed to evaluate the effect of irradiation on ACT degradation as well as the effect of the material in the absence of irradiation. In none of the cases was there any measurable difference between the inlet and outlet concentrations of the contaminant. For all experimental tests performed, the error bars were based on triplicates of the optimum point, i.e., the material that presented the best photocatalytic activity. The increase in the platinum content increased the photocatalytic activity of the material. As shown in Figure 6a, under the same operating conditions (space time of 1 h), the material without platinum exhibited 27% ACT degradation, while the material containing 0.25% Pt showed 81.5% of degradation.

The improved activity of the doped material is related to the presence of PtO_2 and platinum metal [43,44,50]. As shown in the HRTEM of the material (Figure 5d), the close contact between TiO_2 and PtO_2 allows the formation of an effective heterojunction type II [52].

In addition to the effect of PtO_2, Pt^0 nanoparticles are also significant for enhancing the photocatalytic activity of the material. Pt^0 has a work function value of 5.93 eV, while that of TiO_2 is 4.6–4.7 eV [24,27]. The work function is defined as the energy required to remove an electron from the Fermi energy level into the vacuum. Based on stability, if the semiconductor (TiO_2) and the metal (platinum) are in direct contact, there will be a continuous flow of electrons from the material with the lowest (TiO_2) to the material with the highest work function (platinum) until the Fermi energy reaches a constant

equilibrium value for both [52]. This results in the formation of a potential barrier called the Schottky barrier, which works as an electron trap, as the negative charges cannot return to the semiconductor due to this barrier [27,29,53,54]. Therefore, the Schottky barrier prevents the recombination of photogenerated charges and increases the lifetime of the photogenerated electrons, which supports that Pt^0 nanoparticles (NPs) also favorably affect the photocatalytic efficiency of the material [28].

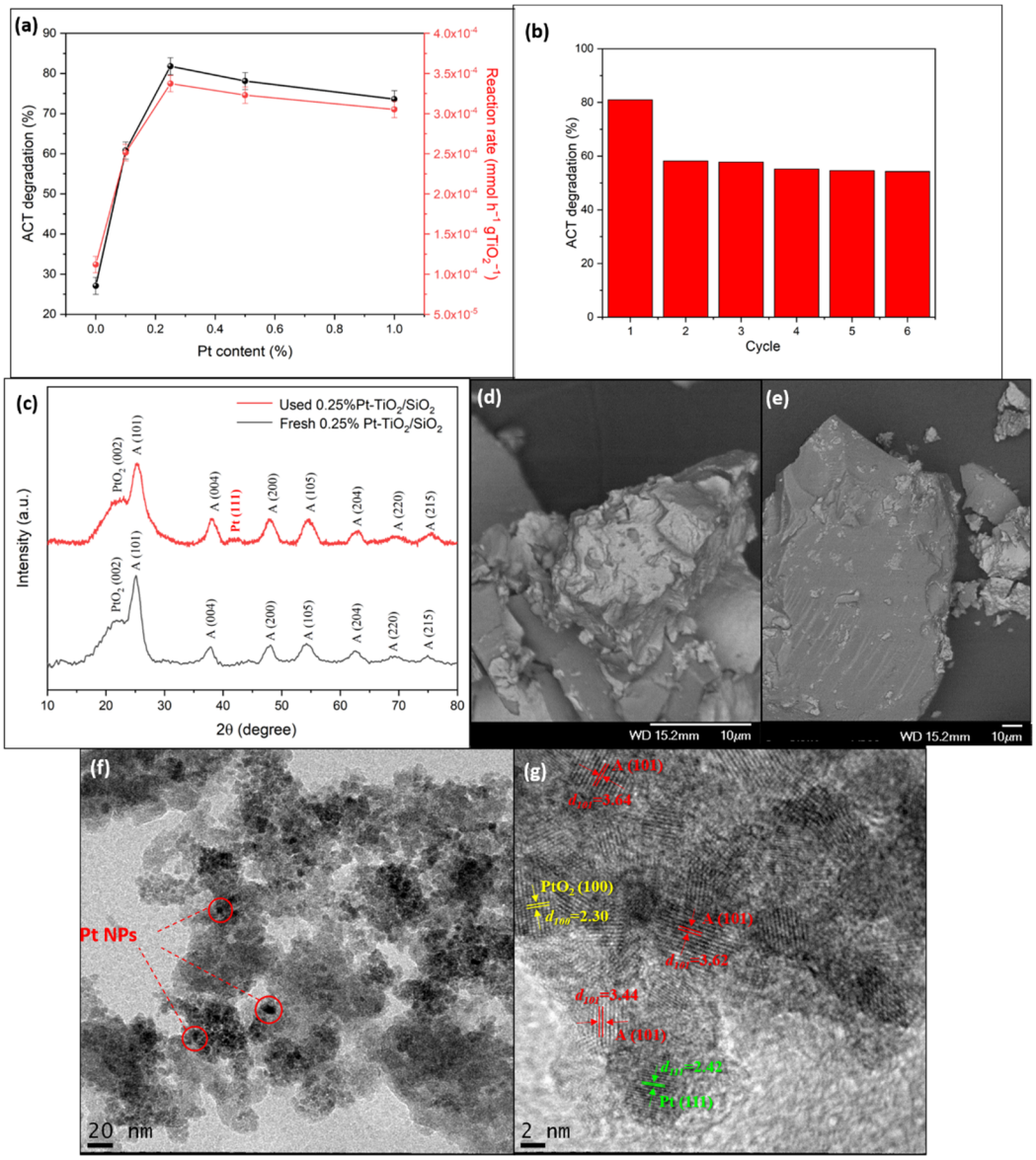

Figure 6. (**a**) Photocatalytic activity of TiO_2/SiO_2 samples with different Pt contents (ACT inlet concentration, 0.033 mmol L^{-1}; volumetric flow rate, 3 mL h^{-1}, space time, 1 h. Error bars are based on triplicates of the optimum point). (**b**) Evaluation of the stability of 0.25%Pt-TiO_2/SiO_2 under continuous operation for six reuse cycles. (**c**) XRD diffractograms of fresh and reused materials. (**d**,**e**) SEM images of reused material. (**f**,**g**) TEM and HRTEM images of reused material.

Finally, it was found that mass contents greater than 0.25% of Pt in the material led to a slight reduction in the catalyst activity. It appears that excessive content of platinum species may block the TiO_2 from being irradiated, resulting in a decrease in photocatalytic activity [17].

The stability of the material 0.25%Pt-TiO_2/SiO_2 was assessed through six successive reuse cycles for 60 min in the continuous fixed-bed photoreactor. The irradiation source was

turned on after 1 h to stabilize the reaction system. Subsequently, the irradiation source was turned on and samples corresponding to consecutive cycles of reuse were collected every 60 min, considering the residence time of 1 h. The ACT removal was reduced from 81% to 57% after six cycle times, which shows that the material still has a good photocatalytic activity, validating the photocatalyst stability. As shown in Figure 6c–g, XRD, SEM, and TEM analyses were conducted to evaluate both fresh and used photocatalysts.

According to XRD diffractograms, the composition of the material was subtly changed during the photocatalytic reaction cycles. The used sample contained an additional peak at 2θ = 40.9°, which is indexed to the (111) plane of face centered cubic (FCC) structure of platinum (JCPDS Card 04-0802). It suggests that during the photodegradation tests, the Pt^{2+} ions from the PtO_2 particles were partially photo-reduced to Pt^0 [27].

The SEM images of the catalyst after reuse were similar to those from fresh samples, presenting TiO_2 crystals both in agglomerated form and supported on silica gel, which suggests it is unlikely that the decrease in photoactivity of the material after reuse cycles is related to leaching of Pt from the synthesized catalyst. The TEM and HRTEM images showed well-defined dark nanoparticles, typical of Pt NPs, which were not observed in the TEM images of fresh catalyst. The HRTEM figures exhibited d-spacing corresponding to PtO_2 (100) and Pt (111) of 2.30 and 2.42 Å, respectively. It is worth mentioning that since the d-spacing values presented in Figure are very close, the authors are not able to assert with certainty to which of the two compounds the d-spacing found refers.

From the results of the characterization analysis, it suggests that the reuse cycles resulted in the photoreduction of PtO_2 to Pt^0 and, consequently, a new mechanism of photocatalytic degradation since PtO_2 and Pt act distinctly on the photocatalytic activity. This may explain the decrease in photoactivity of the catalyst after the reuse cycles.

3.2.2. Effect of Operational Parameters

Experiments were performed varying the volumetric flow rate in the range of 3–12 mL h^{-1} to evaluate the effect of volumetric flow rate on acetaminophen (ACT) removal (Figure 7a). Residence time and mass transfer limitations have opposite effects on ACT conversion when varying the flow rate. The increase in volumetric flow rate benefits the mass transfer and reduces the concentration gradient between the surroundings and the surface of the photocatalyst. On the other hand, increasing the flow rate reduces the residence time in the reactor, thus reducing the contact time between the organic contaminant molecules and the catalyst surface and resulting in a reduction in its degradation [35,40]. Figure 7a shows that although the increase in flow rate led to a reduction in the overall steady-state conversion of ACT, the degradation rate increased.

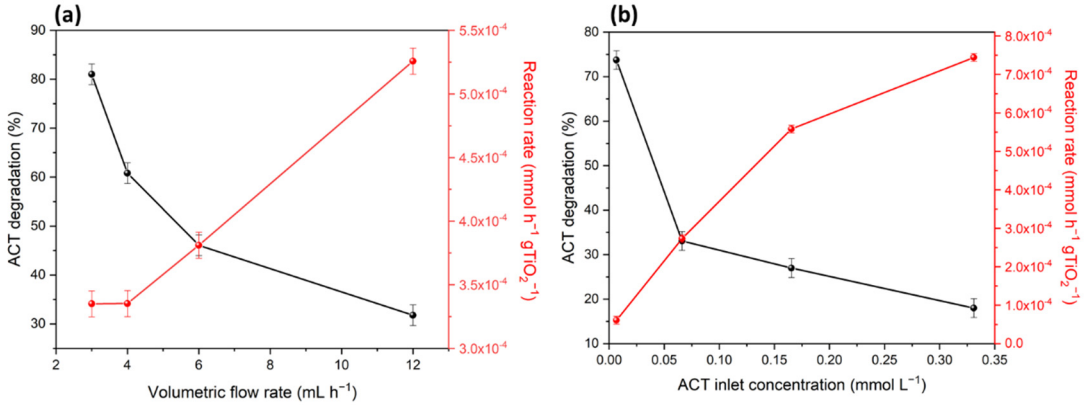

Figure 7. (**a**) Photocatalytic activity of the 0.25%Pt-TiO_2/SiO_2 material for different volumetric flow rates. Error bars are based on triplicates of the optimum point. (**b**) Photocatalytic activity of the 0.25%Pt-TiO_2/SiO_2 material for different ACT inlet concentrations. Error bars are based on triplicates of the optimum point).

Figure 7b shows that increasing the inlet concentration of ACT reduced the steady-state conversion achieved but increased the reaction rate. Since the photocatalytic reaction steps occurs at active sites located on the catalyst surface, if all these sites are already occupied, an increase in the pollutant concentration will reduce ACT degradation. Furthermore, the generation and migration of electron–hole pairs and ACT oxidation by radicals occur in sequence [40]. As the degradation rate increases linearly with the concentration, it is suggested that photocatalytic reactions dominate the process since the number of electron–hole pairs generated exceeds the number of adsorbed contaminant molecules [17].

The degradation kinetics can be further explored assuming that the reactor can be described by a packed-bed reactor (PBR) model. The application of the mass conservation principle for ACT gives [55]:

$$\frac{dF_{ACT}}{dW} = -r \tag{4}$$

where F_{ACT} is the molar flowrate of ACT (mol h^{-1}), W is the catalyst mass (g), and r is the degradation rate. If the degradation reactions proceed with a pseudo-first-order kinetics, whereby $r = -k' C_{ACT}$, integration of Equation (3) yields:

$$k' = \frac{F_{ACT,0}}{W * C_0} \int_0^{X_{ACT}} \frac{dX_{ACT}}{(1 - X_{ACT})} \tag{5}$$

where k' is the pseudo-first-order degradation rate constant (L h^{-1} g^{-1}), C_0 is the inlet ACT concentration (mol L^{-1}), and X_{ACT} is the steady-state conversion. Solving the definite integral yields an expression for k' as a function of the obtained conversion for each C_0 and the main operation parameters, i.e., the flow rate (v_0, L h^{-1}), and the mass of catalyst used as

$$k' = \frac{v_0}{W} \ln(1 - X_{ACT}) \tag{6}$$

The calculated k' are used to evaluate the initial degradation rate, $r_{ACT,0} = k' C_0$ (mol g^{-1} h^{-1}), which is plotted against the inlet concentration of ACT, as shown in Figure 8.

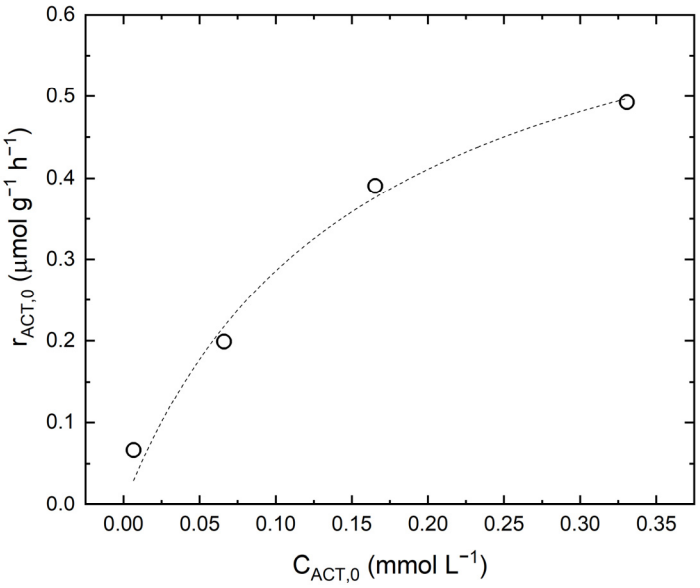

Figure 8. Initial degradation rate of ACT as a function of its inlet concentration. The dashed line represents a Langmuirian fit (R^2 = 0.982).

The data can be fitted to a Langmuir–Hinshelwood kinetics [56,57], where the kinetic contributions of the chemical reaction (k_p) and the adsorption equilibrium (K) can be distinguished:

$$r_{ACT,0} = \frac{k_p K C_0}{1 + K C_0} \tag{7}$$

In the dataset studied, the application of this model was successful (R^2 = 0.982), yielding a specific degradation rate k_p = (7.31 ± 1.17) × 10^{-1} μmol g^{-1} h^{-1} and K = (6.41 ± 2.36) × 10^3 L mol^{-1}. Table 2 summarizes the results.

Table 2. Summary of the kinetic parameters obtained for ACT degradation on 0.25%Pt-TiO_2/SiO_2 in a continuous fixed-bed microreactor (v_0 = 3 mL h^{-1}; space time = 1 h).

C_0 (mg L^{-1})	k' (L g^{-1} h^{-1})	$-r_{ACT,0}$ (μmol g^{-1} h^{-1})	k_p (μmol g^{-1} h^{-1})	K (L mol^{-1})
			0.731	6.41×10^3
1	1.00×10^{-2}	0.067		
10	3.01×10^{-3}	0.199		
25	2.36×10^{-3}	0.390		
50	1.49×10^{-3}	0.492		

3.3. Photocatalytic Mechanism

Figure 9a shows a proposed photocatalytic mechanism for the 0.25%Pt-TiO_2/SiO_2 catalyst based on the characterization analysis and degradation assays performed in this work. The valence and conduction bands of TiO_2 and PtO_2 were calculated through Equations (8) and (9), where E_{VB}, E_{CB}, E_g, E^e, and χ are the valence and conduction bands, the band gap energy, the energy of free electron (~4.5 eV), and the electronegativity of the materials, respectively [46]. The electronegativity of TiO_2 is 4.44 eV and of PtO_2 is 5.06 eV. The band gap value of PtO_2 was obtained from the literature (1.8 eV) [58], and that of TiO_2 was obtained from the Tauc's plot of the pure synthesized material (3.20 eV). Finally, the VB and CB values of TiO_2 were found to be 2.90 and −0.22 eV, respectively, while the VB of PtO_2 was estimated as 1.46 eV and the CB as −0.33 eV.

$$E_{VB} = \chi - E^e + 0.5E_g \quad (8)$$

$$E_{CB} = E_{VB} - E_g \quad (9)$$

As already mentioned, the direct contact of TiO_2 with PtO_2 promoted the formation of a type II heterojunction. A spatial charge zone is formed at the interface of semiconductor materials as a result of charge carrier migration at the semiconductor-semiconductor heterojunction [52]. As the e^-/h^+ pairs migrate through this region, an internal electric field is generated, which causes electrons and holes to flow in opposite directions. Consequently, there is a separation of the photo-generated charges, as electrons are transferred to the conduction band of the semiconductor (TiO_2), which has a lower potential energy, while the positive holes migrate to the valence band of the semiconductor (PtO_2) in order to neutralize the charge balance [52,59,60].

The electrons will diffuse until the thermal equilibrium state is reached in the heterojunctions [31,52]. However, when the material is irradiated, the electrons in the conduction band leave the thermal equilibrium state. Therefore, the charge carrier becomes driven by the potential barriers created. A Schottky barrier is formed between Pt^0/PtO_2 phase junction and TiO_2, which hinders the electron flow between the CBs of PtO_2 and TiO_2. Thus, it is clear that the heterojunction enhanced the charge separation in TiO_2, but for PtO_2, there is an accumulation of positive holes in the VB and electrons in the CB [59].

Figure 9b shows the comparison of the PL emission spectra of TiO_2/SiO_2 and Pt-TiO_2/SiO_2 and supports the mechanism suggested in Figure 9a. In the PL spectra (Figure 9b), all the composite materials show the characteristic peaks of TiO_2 prominently at 415 and 437 and a shoulder at 463 nm. The emission band at 415 nm corresponds to the indirect band-to-band recombination across the band gap. The emission at 437 nm is due to the free exciton emission of TiO_2, and the shoulder at 463 nm resembles oxygen vacancies present on the surface. The higher intensity of PL spectra of Pt-modified material may be attributed to a substantial increase in the photogenerated charges since, while only the TiO_2 absorbs a minor fraction of the solar spectrum (~300–400 nm), PtO_2 NPs also absorb visible light, as shown

by the PtO_2 band gap energy of 1.8 eV. If there is a greater number of photogenerated e^-/h^+ pairs, consequently, there will be a greater intensity in the emission of the present charges present through the mechanisms mentioned above, as indicated by the PL spectrum. The high photocatalytic activity of the Pt-TiO_2/SiO_2 material can be attributed to the significant increase in the number of photogenerated charges.

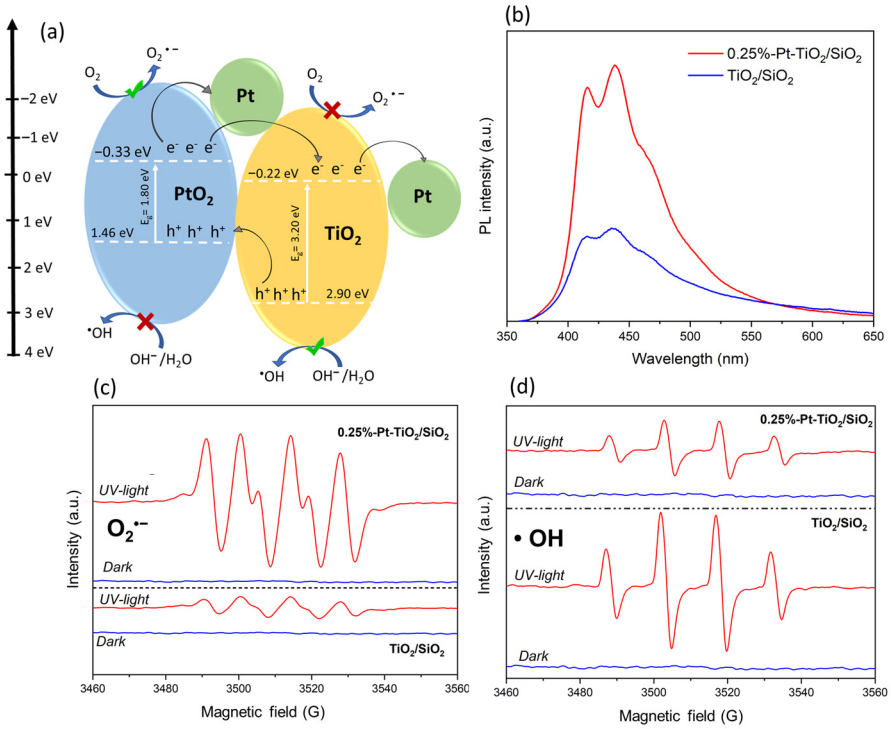

Figure 9. (**a**) Proposed photocatalytic mechanism; (**b**) PL spectra; (**c**) results of $O_2^{\bullet -}$ EPR measurements; (**d**) results of HO• EPR measurements.

In order to deeply investigate the photocatalytic degradation mechanism of ACT under simulated sunlight, the role of oxidizing species was investigated through extra experiments using radical scavengers. Additional runs were conducted using 1,4-hydroquinone, tert-butanol (TBA), potassium iodine (KI), and formic acid as quenchers at initial concentration of 0.02 mol L^{-1} [46]. All experiments were performed with the 0.25%Pt-TiO_2/SiO_2 catalyst, which showed the best photocatalytic activity. 1,4-hydroquinone is known to be a good $O_2^{\bullet -}$ scavenger ($k = 1.6 \times 10^7$ L mol^{-1} s^{-1}) although it can also scavenge •OH radicals ($k = 2.1 \times 10^{10}$ L mol^{-1} s^{-1}) [61]. In turn, TBA is generally used as •OH quencher ($k = 4.2–7.6 \times 10^8$ L mol^{-1} s^{-1}) [62]. KI is employed as an h^+ scavenger since iodine donates e^- to the h^+ in semiconductor materials [62], while formic acid can also scavenge h^+ [62,63] although it can react with •OH with a high-rate constant ($k = 1.2 \times 10^8$ L mol^{-1} s^{-1}) [64]. Thus, in the absence of scavengers, a steady-state ACT removal of 81.5% was obtained, while it decreased to 58.7% with TBA, 44.9% with formic acid, 30.8% with KI, and about 0.0% with 1,4-hydroquinone. These results indicate that the removal of ACT using the 0.25%Pt-TiO_2/SiO_2 catalyst is driven by the reactive species: $O_2^{\bullet -} > h^+ >$ •OH.

EPR spin-trapping experiments for Pt-TiO_2/SiO_2 and TiO_2/SiO_2 were carried out in different reaction media aiming to further investigate the role of reactive species. DMPO was used as a spin-trapping agent to identify the radical species involved in the photocatalytic processes using the synthesized materials [65–67]. To identify hydroxyl radicals, 1.5 mg samples of bare TiO_2/SiO_2 and 0.25%Pt-TiO_2/SiO_2 were placed in vials containing 1.5 mL of a 50 mmol L^{-1} aqueous DMPO solution. The solutions were irradiated at the same irradiance used in the degradation experiments. The solutions were analyzed immediately after the addition of DMPO (in the dark) and after 20 min of irradiation to obtain

the EPR spectra. Then, the superoxide radical anion was determined in a similar way but using 1.5 mL of a 100 mmol L^{-1}.

The results obtained by the EPR analysis shown in Figure 9c,d also support the mechanism suggested in Figure 9a. Regarding the experiments involving hydroxyl radicals, the Pt-TiO_2/SiO_2 material promoted less generation of this radical than TiO_2/SiO_2, suggesting that the h^+ are indeed flowing to the valence band of PtO_2, for which a potential of 1.46 eV was calculated. As this value is lower than the standard reduction potential of the half reactions $HO^{\bullet}/H_2O$ (2.72 eV vs. NHE) and $HO^{\bullet}/OH^-$ (2.40 eV vs. NHE) [19,46], the positive holes in VB of PtO_2 are not able to promote the generation of hydroxyl radicals from water and hydroxide anions. It is worth mentioning that the actual one-electron reduction potentials may be slightly different from the reference values, which are based on standard conditions (temperature and species activities).

Meanwhile, tests involving the superoxide radical showed that, while the TiO_2/SiO_2 catalyst presented a signal intensity close to the superoxide-related noise, the Pt-TiO_2/SiO_2 signal presented an intensity substantially higher, which suggests that the Schottky barrier effectively prevented the flow of electrons to the CB of TiO_2. These results thus support that the conduction band potential of PtO_2 (−0.33 eV) is enough to reduce O_2 to $O_2^{\bullet-}$ ($O_2/O_2^{\bullet-}$: −0.33 eV vs. NHE), while the CB potential of TiO_2 (−0.22 eV) [19,46] is more positive than that of the half reaction $O_2/O_2^{\bullet-}$. It is worth mentioning that in addition to the synergistic effect between semiconductors, it is also proposed that they also act independently in the reaction as co-catalysts. In this sense, the activity of TiO_2 is mainly driven by the formation of hydroxyl radicals, while the activity of PtO_2 by superoxide radicals [58].

4. Conclusions

In this work, TiO_2/SiO_2 photocatalysts coupled to PtO_2 and Pt simultaneously with different Pt contents were successfully synthesized. The catalysts presented heterogeneous geometries, with 20 nm TiO_2 agglomerates and ~10 nm PtO_2 particles adhering to the TiO_2 surface, allowing the formation of a heterojunction between these two materials. The photocatalytic efficiency of the materials was highly influenced by the Pt content. Acetaminophen (ACT) degradation was enhanced as the Pt content increased, reaching a maximum degradation of 81.5% for the material containing 0.25% Pt. At higher Pt contents, however, the photocatalytic activities of the synthesized materials were suppressed. Stability tests showed that the catalyst maintained a stable ACT degradation of 57.0% after six cycles of reuse. Characterization analyses of the reuse material suggested that the Pt^{4+} of PtO_2 was partially photoreduced to metallic Pt. The effect of operational parameters in the continuous flat plate reactor revealed that as the volumetric flow rate increased, the overall ACT degradation was reduced, and the degradation rate increased, implying that mass transfer is the main driven effect. Likewise, increasing the ACT inlet concentration led to a reduction in degradation and to an increase in the degradation rate. EPR spin-trapping experiments demonstrated that both hydroxyl and superoxide radicals species participate in ACT degradation using the 0.25%Pt-TiO_2/SiO_2 photocatalyst. However, due to the formed heterojunction and the Schottky barrier, the modification of the material with platinum induced an increase in the generation of superoxide radicals, while there was a lower generation of hydroxyl radicals. This was supported by the tests carried out with scavengers, which showed that the ACT degradation using the 0.25%Pt-TiO_2/SiO_2 catalyst was determined by the reactive species: $O_2^{\bullet-} > h^+ > {}^{\bullet}OH$. Furthermore, the photoluminescence emission spectrum suggested an increase in photogenerated charges in the Pt-modified material. Finally, the results indicate that the materials synthesized in this work are attractive option for removing organic contaminants using a continuous system and solar light radiation.

Author Contributions: C.d.A.G., conceptualization, methodology, validation, formal analysis, investigation, writing—original draft, and visualization; L.T.B., methodology and formal analysis; P.H.P., methodology, validation, formal analysis, investigation, and writing; L.O., formal analysis, investigation, and visualization; O.R., formal analysis, investigation, and visualization; D.G., investigation, review, and supervision; B.R., formal analysis, investigation, writing—original draft, and visualization; A.C.S.C.T., conceptualization, validation, resources, writing—original draft, writing—review and editing, supervision, and funding acquisition. All authors have read and agreed to the published version of the manuscript.

Funding: The authors express their gratitude to the São Paulo Research Foundation (FAPESP, grant no. 2019/24158-9, 2018/2171-6, 2021/10919-8 and 2022/12331-0), to the Brazilian National Council for Scientific and Technological Development (CNPq, grant no. 131467/2017-4) and to the Coordination for the Improvement of Higher Education Personnel—Brazil (CAPES)—Finance Code 001. Moreover, this research used facilities of the Brazilian Nanotechnology National Laboratory (LNNano), part of the Brazilian Center for Research in Energy and Materials (CNPEM), a private non-profit organization under the supervision of the Brazilian Ministry for Science, Technology, and Innovations (MCTI).

Acknowledgments: This study was financed in part by the Coordenação de Aperfeiçoamento de Pessoal de Nível Superior—Brasil (CAPES)—Finance Code 001. The authors also express their gratitude to the National Council of Scientific and Technological Development (CNPq, Brazil, grant #311230/2020-2) and to the São Paulo Research Foundation (FAPESP, grants #2016/00953-6, #2018/21271-6 and #2019/24158-9) for the financial support. Additionally, this research used facilities of the Brazilian Nanotechnology National Laboratory (LNNano), part of the Brazilian Centre for Research in Energy and Materials (CNPEM), a private non-profit organization under the supervision of the Brazilian Ministry for Science, Technology, and Innovations (MCTI). The Ângela Albuquerque Teixeira Neto staff is acknowledged for the assistance during the experiments (XPS-20220414).

Conflicts of Interest: The authors declare no conflict of interest.

References

1. Paumo, H.K.; Dalhatou, S.; Katata-Seru, L.M.; Kamdem, B.P.; Tijani, J.O.; Vishwanathan, V.; Kane, A.; Bahadur, I. TiO_2 Assisted Photocatalysts for Degradation of Emerging Organic Pollutants in Water and Wastewater. *J. Mol. Liq.* **2021**, *331*, 115458. [CrossRef]
2. Leyva, E.; Moctezuma, E.; Baines, K.M.; Noriega, S.; Zarazua, E. A Review on Chemical Advanced Oxidation Processes for Pharmaceuticals with Paracetamol as a Model Compound. Reaction Conditions, Intermediates and Total Mechanism. *Curr. Org. Chem.* **2017**, *22*, 2–17. [CrossRef]
3. Ikehata, K.; Jodeiri Naghashkar, N.; Gamal El-Din, M. Degradation of Aqueous Pharmaceuticals by Ozonation and Advanced Oxidation Processes: A Review. *Ozone Sci. Eng.* **2006**, *28*, 353–414. [CrossRef]
4. Rivera-Utrilla, J.; Sánchez-Polo, M.; Ferro-García, M.Á.; Prados-Joya, G.; Ocampo-Pérez, R. Pharmaceuticals as Emerging Contaminants and Their Removal from Water. A Review. *Chemosphere* **2013**, *93*, 1268–1287. [CrossRef]
5. Freyria, F.S.; Geobaldo, F.; Bonelli, B. Nanomaterials for the Abatement of Pharmaceuticals and Personal Care Products from Wastewater. *Appl. Sci.* **2018**, *8*, 170. [CrossRef]
6. Taoufik, N.; Boumya, W.; Achak, M.; Sillanpää, M.; Barka, N. Comparative Overview of Advanced Oxidation Processes and Biological Approaches for the Removal Pharmaceuticals. *J. Environ. Manag.* **2021**, *288*, 112404. [CrossRef]
7. Bousiakou, L.G.; Mohsin, K.; Lianos, P.; Fatani, A.J.; Kalkani, E.; Karikas, G.A. Wastewater Treatment Technologies in the Degradation of Hormones and Pharmaceuticals with Focus on TiO_2 Technologies. *Pharmakeftiki* **2013**, *25*, 37–48.
8. Stackelberg, P.E.; Furlong, E.T.; Meyer, M.T.; Zaugg, S.D.; Henderson, A.K.; Reissman, D.B. Persistence of Pharmaceutical Compounds and Other Organic Wastewater Contaminants in a Conventional Drinking-Water-Treatment Plant. *Sci. Total Environ.* **2004**, *329*, 99–113. [CrossRef] [PubMed]
9. Chau, J.H.F.; Lai, C.W.; Leo, B.F.; Juan, J.C.; Johan, M.R. Advanced photocatalytic degradation of acetaminophen using Cu2O/WO3/TiO2 ternary composite under solar irradiation. *Catal. Commun.* **2022**, *163*, 106396. [CrossRef]
10. Montagner, C.C.; Sodré, F.F.; Acayaba, R.D.; Vidal, C.; Campestrini, I.; Locatelli, M.A.; Pescara, I.C.; Albuquerque, A.F.; Umbuzeiro, G.A.; Jardim, W.F. Ten Years-Snapshot of the Occurrence of Emerging Contaminants in Drinking, Surface and Ground Waters and Wastewaters from São Paulo State, Brazil. *J. Braz. Chem. Soc.* **2019**, *30*, 614–632. [CrossRef]
11. Guerra, P.; Kim, M.; Shan, A.; Alaee, M.; Smyth, S.A. Occurrence and Fate of Antibiotic, Analgesic/Anti-Inflammatory, and Antifungal Compounds in Five Wastewater Treatment Processes. *Sci. Total Environ.* **2014**, *473*, 235–243. [CrossRef] [PubMed]
12. Yang, L.; Yu, L.E.; Ray, M.B. Degradation of Paracetamol in Aqueous Solutions by TiO_2 Photocatalysis. *Water Res.* **2008**, *42*, 3480–3488. [CrossRef]
13. Kanakaraju, D.; Glass, B.D.; Oelgemöller, M. Advanced Oxidation Process-Mediated Removal of Pharmaceuticals from Water: A Review. *J. Environ. Manag.* **2018**, *219*, 189–207. [CrossRef] [PubMed]

14. Abdel Salam, M.; Mokhtar, M.; Albukhari, S.M.; Baamer, D.F.; Palmisano, L.; Jaremko, M.; Abukhadra, M.R. Synthesis and Characterization of Green ZnO@polynaniline/Bentonite Tripartite Structure (G.Zn@PN/BE) as Adsorbent for As (V) Ions: Integration, Steric, and Energetic Properties. *Polymers* **2022**, *14*, 2329. [CrossRef] [PubMed]
15. Al-Soihi, A.S.; Alsulami, Q.A.; Mostafa, M.M.M. Amalgamated Titanium Oxide-Carbon Hollow Sphere/Nickel-Layered Double Hydroxide as an Efficient Photocatalyst for the Degradation of Methyl Orange. *Catalysts* **2022**, *12*, 1200. [CrossRef]
16. Baaloudj, O.; Nasrallah, N.; Kebir, M.; Khezami, L.; Amrane, A.; Assadi, A.A.; Schneider, J.; Matsuoka, M.; Takeuchi, M.; Zhang, J.; et al. A comparative study of ceramic nanoparticles synthesized for antibiotic removal: Catalysis characterization and photocatalytic performance modeling. *Environ. Sci. Pollut. Res.* **2021**, *28*, 13900–13912. [CrossRef]
17. Carp, O.; Huisman, C.L.; Reller, A. Photoinduced Reactivity of Titanium Dioxide. *Prog. Solid State Chem.* **2004**, *32*, 33–177. [CrossRef]
18. Shahbazi, R.; Payan, A.; Fattahi, M. Preparation, Evaluations and Operating Conditions Optimization of Nano TiO_2 over Graphene Based Materials as the Photocatalyst for Degradation of Phenol. *J. Photochem. Photobiol. A Chem.* **2018**, *364*, 564–576. [CrossRef]
19. Gusmão, C.A.; Palharim, P.H.; Ramos, B.; Teixeira, A.C.S.C. Enhancing the Visible-Light Photoactivity of Silica-Supported TiO_2 for the Photocatalytic Treatment of Pharmaceuticals in Water. *Environ. Sci. Pollut. Res.* **2021**, 42215–42230. [CrossRef]
20. Pelaez, M.; Nolan, N.T.; Pillai, S.C.; Seery, M.K.; Falaras, P.; Kontos, A.G.; Dunlop, P.S.M.; Hamilton, J.W.J.; Byrne, J.A.; O'Shea, K.; et al. A Review on the Visible Light Active Titanium Dioxide Photocatalysts for Environmental Applications. *Appl. Catal. B Environ.* **2012**, *125*, 331–349. [CrossRef]
21. Ibrahim, N.S.; Leaw, W.L.; Mohamad, D.; Alias, S.H.; Nur, H. A Critical Review of Metal-Doped TiO_2 and Its Structure–Physical Properties–Photocatalytic Activity Relationship in Hydrogen Production. *Int. J. Hydrog. Energy* **2020**, *45*, 28553–28565. [CrossRef]
22. Akpan, U.G.; Hameed, B.H. The Advancements in Sol-Gel Method of Doped-TiO_2 Photocatalysts. *Appl. Catal. A Gen.* **2010**, *375*, 1–11. [CrossRef]
23. Shukla, S.; Pandey, H.; Singh, P.; Tiwari, A.K.; Baranwal, V.; Pandey, A.C. Synergistic Impact of Photocatalyst and Dopants on Pharmaceutical-Polluted Waste Water Treatment: A Review. *Environ. Pollut. Bioavailab.* **2021**, *33*, 347–364. [CrossRef]
24. Fang, M.; Tan, X.; Liu, Z.; Hu, B.; Wang, X. Recent Progress on Metal-Enhanced Photocatalysis: A Review on the Mechanism. *Research* **2021**, *2021*, 794329. [CrossRef] [PubMed]
25. Dey, D.; Halder, N.; Misra, K.P.; Chattopadhyay, S.; Jain, S.K.; Bera, P.; Kumar, N.; Mukhopadhyay, A.K. Systematic Study on the Effect of Ag Doping in Shaping the Magnetic Properties of Sol-Gel Derived TiO_2 Nanoparticles. *Ceram. Int.* **2020**, *46*, 27832–27848. [CrossRef]
26. Mehrali-Afjani, M.; Nezamzadeh-Ejhieh, A.; Aghaei, H. A Brief Study on the Kinetic Aspect of the Photodegradation and Mineralization of BiOI-Ag_3PO_4 towards Sodium Diclofenac. *Chem. Phys. Lett.* **2020**, *759*, 137873. [CrossRef]
27. Khan, M.R.; Chuan, T.W.; Yousuf, A.; Chowdhury, M.N.K.; Cheng, C.K. Schottky Barrier and Surface Plasmonic Resonance Phenomena towards the Photocatalytic Reaction: Study of Their Mechanisms to Enhance Photocatalytic Activity. *Catal. Sci. Technol.* **2015**, *5*, 2522–2531. [CrossRef]
28. Kumari, P.; Bahadur, N.; Kong, L.; O'Dell, L.A.; Merenda, A.; Dumée, L.F. Engineering Schottky-like and Heterojunction and Heterojunction Materials for Enhanced Photocatalysis Performance—A review. *Mater. Adv.* **2022**, *3*, 2309–2323. [CrossRef]
29. Li, P.; Guo, J.; Ji, X.; Xiong, Y.; Lai, Q.; Yao, S.; Zhu, Y.; Zhang, Y.; Xiao, P. Construction of Direct Z-Scheme Photocatalyst by the Interfacial Interaction of WO_3 and SiC to Enhance the Redox Activity of Electrons and Holes. *Chemosphere* **2021**, *282*, 130866. [CrossRef]
30. Zhang, F.; Wang, M.; Zhu, X.; Hong, B.; Wang, W.; Qi, Z.; Xie, W.; Ding, J.; Bao, J.; Sun, S.; et al. Effect of Surface Modification with H_2S and NH_3 on TiO_2 for Adsorption and Photocatalytic Degradation of Gaseous Toluene. *Appl. Catal. B Environ.* **2015**, *170*, 215–224. [CrossRef]
31. Parayil, S.K.; Kibombo, H.S.; Wu, C.M.; Peng, R.; Kindle, T.; Mishra, S.; Ahrenkiel, S.P.; Baltrusaitis, J.; Dimitrijevic, N.M.; Rajh, T.; et al. Synthesis-Dependent Oxidation State of Platinum on TiO_2 and Their Influences on the Solar Simulated Photocatalytic Hydrogen Production from Water. *J. Phys. Chem. C* **2013**, *117*, 16850–16862. [CrossRef]
32. Murcia, J.J.; Hidalgo, M.C.; Navío, J.A.; Vaiano, V.; Sannino, D.; Ciambelli, P. Cyclohexane Photocatalytic Oxidation on Pt/TiO_2 Catalysts. *Catal. Today* **2013**, *209*, 164–169. [CrossRef]
33. Ren, X.N.; Hu, Z.Y.; Jin, J.; Wu, L.; Wang, C.; Liu, J.; Liu, F.; Wu, M.; Li, Y.; Van Tendeloo, G.; et al. Cocatalyzing Pt/PtO Phase-Junction Nanodots on Hierarchically Porous TiO_2 for Highly Enhanced Photocatalytic Hydrogen Production. *ACS Appl. Mater. Interfaces* **2017**, *9*, 29687–29698. [CrossRef]
34. Sundar, K.P.; Kanmani, S. Chemical Engineering Research and Design Progression of Photocatalytic Reactors and It's Comparison: A Review. *Chem. Eng. Res. Des.* **2020**, *154*, 135–150. [CrossRef]
35. Van Gerven, T.; Mul, G.; Moulijn, J.; Stankiewicz, A. A Review of Intensification of Photocatalytic Processes. *Chem. Eng. Process. Process Intensif.* **2007**, *46*, 781–789. [CrossRef]
36. Rincón, G.J.; La Motta, E.J. A Fluidized-Bed Reactor for the Photocatalytic Mineralization of Phenol on TiO_2-Coated Silica Gel. *Heliyon* **2019**, *5*, e01966. [CrossRef] [PubMed]
37. Shi, M.; Hu, N.; Liu, H.; Qian, C.; Lv, C.; Wang, S. Controlled Synthesis of Pt-Loaded Yolk-Shell TiO_2@SiO_2 Nanoreactors as Effective Photocatalysts for Hydrogen Generation. *Front. Mater. Sci.* **2022**, *16*, 220591. [CrossRef]

38. Ramos, B.; Carneiro, J.G.; De, M.; Nagamati, L.I.; Teixeira, A.C.S.C. Development of Intensified Flat-Plate Packed-Bed Solar Reactors for Heterogeneous Photocatalysis. *Environ. Sci. Pollut. Res.* **2021**, *28*, 24023–24033. [CrossRef] [PubMed]
39. Thamaphat, K.; Limsuwan, P.; Ngotawornchai, B. Phase Characterization of TiO_2 Powder by XRD and TEM. *Kasetsart J.* **2008**, *42*, 357–361.
40. Gusmão, C.D.A.; Almeida, L.; Ramos, B.; Gomes, A.; Geraldo, J.; Pacheco, A.; Carlos, A.; Costa, S. Optimization of TiO_2/SiO_2 Photocatalysts in a LED-Irradiated Gas-Solid Photoreactor for Air Treatment. *Chem. Eng. Res. Des.* **2022**, *185*, 223–238. [CrossRef]
41. Bensouici, F.; Souier, T.; Dakhel, A.A.; Iratni, A.; Tala-Ighil, R.; Bououdina, M. Synthesis, Characterization and Photocatalytic Behavior of Ag Doped TiO_2 Thin Film. *Superlattices Microstruct.* **2015**, *85*, 255–265. [CrossRef]
42. Diniz, L.A.; Matsumoto, D.; Carlos, A.; Costa, S. Photocatalytic Degradation of N-Hexane in a Circulating Fl Uidized Bed: An Investigation Based on the Freeboard Entrainment Model. *Catal. Today* **2021**, *361*, 109–116. [CrossRef]
43. Kibombo, H.S.; Wu, C.M.; Peng, R.; Baltrusaitis, J.; Koodali, R.T. Investigation of the Role of Platinum Oxide for the Degradation of Phenol under Simulated Solar Irradiation. *Appl. Catal. B Environ.* **2013**, *136–137*, 248–259. [CrossRef]
44. Valizadeh, A.; Aleshkevych, P.; Najafpour, M.M. Role of Pt and PtO_2 in the Oxygen-Evolution Reaction in the Presence of Iron under Alkaline Conditions. *Inorg. Chem.* **2022**, *61*, 613–621. [CrossRef] [PubMed]
45. Nezamzadeh-Ejhieh, A.; Bahrami, M. Investigation of the photocatalytic activity of supported ZnO–TiO_2 on clinoptilolite nano-particles towards photodegradation of wastewater-contained phenol. *Desalin. Water Treat.* **2015**, *55*, 1096–1104. [CrossRef]
46. Hasse Palharim, P.; Lara Diego dos Reis Fusari, B.; Ramos, B.; Otubo, L.; Carlos Silva Costa Teixeira, A. Effect of HCl and HNO_3 on the Synthesis of Pure and Silver-Based WO3 for Improved Photocatalytic Activity under Sunlight. *J. Photochem. Photobiol. A Chem.* **2021**, *422*, 113550. [CrossRef]
47. Post, P.; Wurlitzer, L.; Maus-Friedrichs, W.; Weber, A.P. Characterization and Applications of Nanoparticles Modified In-Flight with Silica or Silica-Organic Coatings. *Nanomaterials* **2018**, *8*, 530. [CrossRef]
48. Liu, D.; Shen, J.; Xie, Y.; Qiu, C.; Zhang, Z.; Long, J.; Lin, H.; Wang, X. Metallic Pt and PtO2 Dual-Cocatalyst-Loaded Binary Composite 2 RGO-CN. *ACS Sustain. Chem. Eng.* **2021**, *9*, 6380–6389. [CrossRef]
49. Serpone, N. Is the Band Gap of Pristine TiO_2 Narrowed by Anion-and Cation-Doping of Titanium Dioxide in Second-Generation Photocatalysts? *J. Phys. Chem. B* **2006**, *110*, 24287–24293. [CrossRef]
50. Liu, J.; Li, D.; Li, R.; Wang, Y.; Wang, Y.; Fan, C. PtO/Pt^{4+}-BiOCl with Enhanced Photocatalytic Activity: Insight into the Defect-Filled Mechanism. *Chem. Eng. J.* **2020**, *395*, 123954. [CrossRef]
51. Li, Q.; Li, F.T. Recent Advances in Surface and Interface Design of Photocatalysts for the Degradation of Volatile Organic Compounds. *Adv. Colloid Interface Sci.* **2020**, *284*, 102275. [CrossRef]
52. Schneider, J.; Matsuoka, M.; Takeuchi, M.; Zhang, J.; Horiuchi, Y.; Anpo, M.; Bahnemann, D.W. Understanding TiO_2 Photocatalysis Mechanisms and Materials. *Chem. Rev.* **2014**, *114*, 9919–9986. [CrossRef]
53. García-Muñoz, P.; Zussblatt, N.P.; Chmelka, B.F.; de la Peña O'Shea, V.A.; Fresno, F. Production of Hydrogen from Gas-Phase Ethanol Dehydrogenation over Iron-Grafted Mesoporous Pt/TiO_2 Photocatalysts. *Chem. Eng. J.* **2022**, *450*, 138450. [CrossRef]
54. Pu, S.; Hou, Y.; Chen, H.; Deng, D.; Yang, Z.; Xue, S.; Zhu, R.; Diao, Z.; Chu, W. An Efficient Photocatalyst for Fast Reduction of Cr(VI) by Ultra-Trace Silver Enhanced Titania in Aqueous Solution. *Catalysts* **2018**, *8*, 251. [CrossRef]
55. Levenspiel, O. *The Chemical Reactor Omnibook*; Lulu Press: Morrisville, NC, USA, 2013.
56. Ohtani, B. *Photocatalysis by Inorganic Solid Materials: Revisiting Its Definition, Concepts, and Experimental Procedures*, 1st ed.; Elsevier Inc.: Amsterdam, The Netherlands, 2011; Volume 63, ISBN 9780123859044.
57. Valente, J.P.S.; Padilha, P.M.; Florentino, A.O. Studies on the Adsorption and Kinetics of Photodegradation of a Model Compound for Heterogeneous Photocatalysis onto TiO_2. *Chemosphere* **2006**, *64*, 1128–1133. [CrossRef]
58. Yang, Y.; Sugino, O.; Ohno, T. Band gap of β-PtO_2 from first-principles. *AIP Adv.* **2012**, *2*, 022172. [CrossRef]
59. Yang, H. A short review on heterojunction photocatalysts: Carrier transfer behavior and photocatalytic mechanisms. *Mater. Res. Bull.* **2021**, *142*, 111406. [CrossRef]
60. Le, T.H.; Bui, T.T.; Bui, H.V.; Dao, V.D.; Ngoc, L.L.T. TiO_2 Inverse Opals Modified by Ag Nanoparticles: A Synergic effect of Enhanced Visible-Light Absorption and Efficient Charge Separation for Visible-Light Photocatalysis. *Catalysts* **2021**, *11*, 761. [CrossRef]
61. Fónagy, O.; Szabó-Bárdos, E.; Horváth, O. 1, 4-Benzoquinone and 1, 4-hydroquinone based determination of electron and superoxide radical formed in heterogeneous photocatalytic systems. *J. Photochem. Photobiol. A Chem.* **2021**, *407*, 113057. [CrossRef]
62. Schneider, J.T.; Firak, D.S.; Ribeiro, R.R.; Peralta-Zamora, P. Use of scavenger agents in heterogeneous photocatalysis: Truths, half-truths, and misinterpretations. *Phys. Chem. Chem. Phys.* **2020**, *27*, 15723–15733. [CrossRef] [PubMed]
63. Pelaez, M.; Falaras, P.; Likodimos, V.; O'Shea, K.; Armah, A.; Dunlop, P.S.; AnthonyByrne, A.; Dionysiou, D. Use of selected scavengers for the determination of NF-TiO_2 reactive oxygen species during the degradation of microcystin-LR under visible light irradiation. *J. Mol. Catal. A Chem.* **2016**, *425*, 183–189. [CrossRef] [PubMed]
64. Buxton, G.V.; Greenstock, C.L.; Helman, W.P.; Ross, A.B. Critical review of rate constants for reactions of hydrated electrons, hydrogen atoms and hydroxyl radicals (OH/O^-) in aqueous solution. *J. Phys. Chem. Ref. Data* **1988**, *17*, 513–886. [CrossRef]
65. Al-Madanat, O.; Nunes, B.N.; Alsalka, Y.; Hakki, A.; Curti, M.; Patrocinio, A.O.T.; Bahnemann, D.W. Application of EPR Spectroscopy in TiO_2 and Nb_2O_5 Photocatalysis. *Catalysts* **2021**, *11*, 1514. [CrossRef]

66. Dvoranová, D.; Barbieriková, Z.; Brezová, V. Radical Intermediates in Photoinduced Reactions on TiO_2 (An EPR Spin Trapping Study). *Molecules* **2014**, *19*, 17279–17304. [CrossRef] [PubMed]
67. Nie, J.; Schneider, J.; Sieland, F.; Zhou, L.; Xia, S.; Bahnemann, D.W. New Insights into the Surface Plasmon Resonance (SPR) Driven Photocatalytic H_2 Production of Au-TiO_2. *RSC Adv.* **2018**, *8*, 25881–25887. [CrossRef]